Terahertz time-domain spectroscopy of anisotropic complex conductivity tensors in silicon nanowire films

Meehyun Lim, Sung-Jin Choi, Gyu-Seok Lee, Myeong-Lok Seol, Youngwoong Do et al.

Related Articles

Multi-scale graphene patterns on arbitrary substrates via laser-assisted transfer-printing process
Appl. Phys. Lett. 101, 043110 (2012)

Ultrafast third order nonlinear optical response of donor and acceptor codoped and compensated silicon quantum dots
Appl. Phys. Lett. 101, 041112 (2012)

Nanomodification of gold surface by picosecond soft x-ray laser pulse
J. Appl. Phys. 112, 013104 (2012)

Ultrafast laser induced breakdown spectroscopy of electrode/electrolyte interfaces
Appl. Phys. Lett. 100, 234101 (2012)

Application of the Z-scan technique to determine the optical Kerr coefficient and two-photon absorption coefficient of magnetite nanoparticles colloidal suspension
J. Appl. Phys. 111, 113509 (2012)
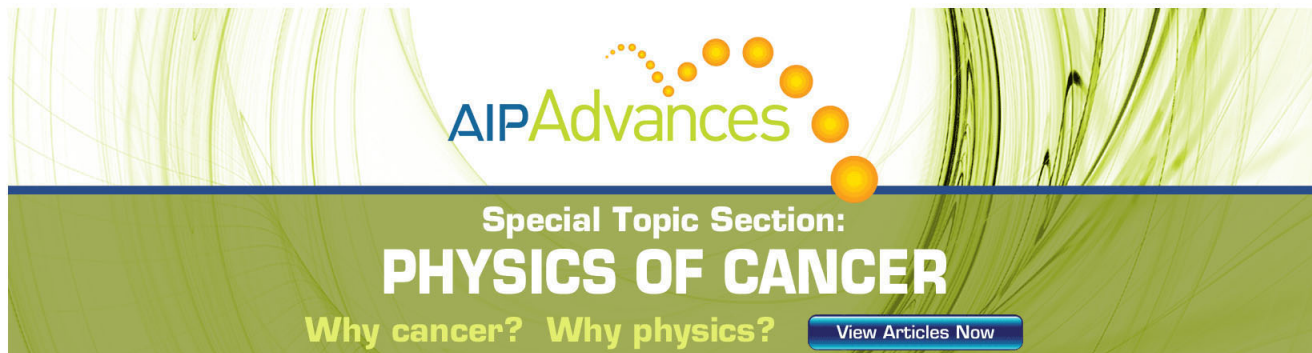
Additional information on Appl. Phys. Lett.

Journal Homepage: http://apl.aip.org/

Journal Information: http://apl.aip.org/about/about_the_journal

Top downloads: http://apl.aip.org/features/most_downloaded

Information for Authors: http://apl.aip.org/authors

Terahertz time-domain spectroscopy of anisotropic complex conductivity tensors in silicon nanowire films

Meehyun Lim,[1] Sung-Jin Choi,[2] Gyu-Seok Lee,[1] Myeong-Lok Seol,[2] Youngwoong Do,[1] Yang-Kyu Choi,[2] and Haewook Han[1,a)]

[1]*Department of Electrical and Computer Engineering, POSTECH, Pohang, Kyungbuk 790-784, Korea*
[2]*Division of Electrical Engineering, School of Electrical Engineering and Computer Science, KAIST, 335 Gwahangno, Yuseong-gu, Daejeon, 305-701, Korea*

The effective complex conductivity tensor of a highly anisotropic, vertically aligned silicon nanowire film was measured by terahertz time-domain spectroscopy. The silicon nanowires were fabricated on a *p*-type silicon substrate by metal-assisted chemical etching, which resulted in a film with uniaxially anisotropic optical properties. The measured terahertz transverse and longitudinal conductivity values were in excellent agreement with the results of calculations based on the Drude-Smith and Lorentz models, respectively. © *2012 American Institute of Physics*. [http://dx.doi.org/10.1063/1.4721490]

Semiconductor nanowires have been studied extensively for various applications in electronics and photonics. Silicon nanowires (SiNWs), in particular, have attracted considerable attention for use in many applications, including functional nanoscale building blocks, thermoelectric power conversion devices, and biochemical sensors.[1–4] Recently, SiNWs have also been applied to the generation of broadband terahertz (THz) pulses.[5] For the THz device applications of SiNWs, a comprehensive understanding of the anisotropic dielectric and transport properties of SiNWs at THz frequencies is important. For various materials, ranging from semiconductor nanowires[6–9] to biomolecules,[10,11] these properties can be effectively determined, in principle, through THz time-domain spectroscopy (TDS). However, conventional THz-TDS has mostly been used to characterize polarization-independent isotropic materials. Although the conventional THz-TDS technique has also been used successfully for the polarization-sensitive measurement of birefringent THz photonic crystal fibers,[12] only a few experimental studies have dealt with the THz spectroscopy of semiconductor nanowires.[6–9]

As semiconductor nanowires are usually fabricated on thick substrates, quantitative analysis of these semiconductor nanowires requires the development of high-precision spectroscopic ellipsometry techniques, which are suitable for the characterization of thin films on thick and opaque substrates with anisotropic optical properties.[17] However, the THz ellipsometry is still in its infancy and has limited accuracy when compared with conventional infrared ellipsometry, mainly because of the lack of high-power THz sources, high-performance THz polarizers, and precise alignment techniques. THz time-domain spectroscopic ellipsometry has previously been used to characterize doped silicon substrates and GaAs thin films,[13–16] and metal nanowires have also been analyzed by THz frequency-domain ellipsometry.[18] However, complete characterization of the complex dielectric tensors of SiNW films has not yet been demonstrated. In this work, we report high-precision THz-TDS characterization of a SiNW film fabricated on a *p*-type silicon wafer. We successfully demonstrate THz-TDS analysis of the effective complex conductivity tensor of the SiNW film. The THz-TDS measurements of the transverse and longitudinal conductivity values of the SiNW film are found to be in excellent agreement with the results of calculations based on the Drude-Smith (DS) and Lorentz models, respectively.

Vertically aligned SiNWs were fabricated on top of *p*-type (100) silicon wafers by metal-assisted chemical etching;[19] the wafers were ~525 μm thick, with a resistivity of 1–10 Ω·cm, corresponding to a carrier density of ~10^{16} cm^{-3}. Prior to the etching process, a thin discontinuous Au layer (thickness of ~7 nm) was deposited on the substrate by thermal evaporation. The sample was then etched in a solution of hydrofluoric acid and hydrogen peroxide (HF (2):H$_2$O$_2$ (1):H$_2$O (7)) under dark conditions at room temperature and was subsequently rinsed in deionized water; finally, the residual Au layer was etched. Figure 1(a) shows the scanning electron microscopy (SEM) images of the SiNW layer; the average diameter and length of the SiNWs are ~90 nm and ~3 μm, respectively. To quantitatively evaluate the effective permittivity tensor of the SiNWs, we used a THz-TDS system in transmission mode. The THz pulse was generated using an InAs wafer pumped by a Ti:sapphire laser with a center wavelength of 800 nm, a pulse width of 100 fs, and a repetition rate of 80 MHz. The THz pulse was focused on the sample using an off-axis parabolic mirror, and the transmitted THz pulse was then detected using a photoconductive antenna fabricated on low-temperature-grown GaAs. The entire THz-TDS system was enclosed in a chamber which was continuously purged with dry air to eliminate THz absorption by the water vapor in the air. The THz-TDS system has a measurable frequency band, ranging from 0.2 THz to 1.5 THz. The incident THz pulse was *p*-polarized with an electric field parallel to the plane of incidence.

For the THz transmission analysis, the SiNW film was modeled as a homogeneous anisotropic thin film, as shown

---

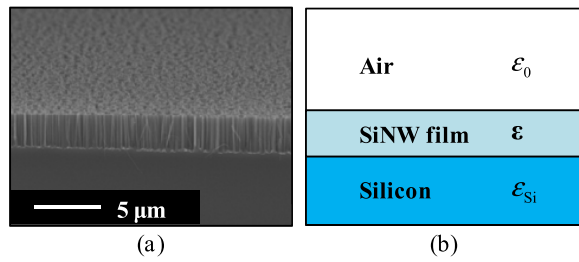a)Author to whom correspondence should be addressed: Electronic mail: hhan@postech.ac.kr.

FIG. 1. (a) SEM images of vertically aligned SiNWs (average diameter: ~90 nm; average length: ~3 μm) on a silicon substrate and (b) equivalent dielectric layers, where **ε** is the effective complex permittivity tensor of the SiNW film, which is regarded as a homogeneous anisotropic medium, and ε_0 and ε_{Si} are the relative permittivities of air and the silicon substrate, respectively.

in Fig. 1(b). In effective medium theory, the macroscopic effective complex permittivity of a mixture is usually determined by the microscopic polarizability or the transport parameters of the inclusions (the SiNWs in this work) along with the mixing parameters, such as the volume fraction and the depolarization factors of the inclusions.[20,21] However, we can also use the macroscopic dispersion models of the effective permittivity,[20] which are directly defined by the macroscopic transport parameters, such as the effective plasma frequency and the relaxation time. The measured transmission coefficients were compared with the calculations to obtain the macroscopic transport parameters using a least-squares method. As will be shown later in the paper, this phenomenological approach results in excellent agreement between the THz measurements and the calculations, without the need for any specific model of the effective medium theory.

The SiNW thin film has highly anisotropic dielectric properties, and the effective complex permittivity tensor is given by $\boldsymbol{\varepsilon} = \varepsilon_t \mathbf{I}_t + \varepsilon_z \mathbf{u}_z \mathbf{u}_z$, where ε_t and ε_z are the transverse and longitudinal complex permittivities, respectively; $\mathbf{I}_t$ is the transverse identity tensor; and $\mathbf{u}_z$ is the surface normal unit vector. The transmission coefficient for an anisotropic film on an isotropic substrate can be found from the Fresnel equation.[21] The measurements and calculations of the THz pulses and spectra transmitted through the SiNW film on a Si substrate at incidence angles (θ) of 0° and 40° are shown in Fig. 2, where we used the single-pass transmission coefficient for the thick Si substrate because the secondary pulses due to multiple reflections are well separated from the primary pulse. The THz pulse for $\theta = 40°$, which is less than the Brewster angle at the air-film interface, has a larger peak amplitude than that for the pulse at normal incidence. Also, a time delay of ~0.3 ps between the peak positions of the THz pulses for incidence angles of 0° and 40° was observed as expected. As shown in Fig. 2, the measurements were in excellent agreement with the results of the calculations in both the time and frequency domains. The effective complex relative permittivity tensor is defined as:

$$\varepsilon(\omega) = \varepsilon_\infty + j\frac{\boldsymbol{\sigma}(\omega)}{\omega \varepsilon_0}, \qquad (1)$$

where ε_∞ is the relative permittivity tensor at high frequencies, ε_0 is the permittivity of free space, and $\boldsymbol{\sigma}(\omega)$ is the
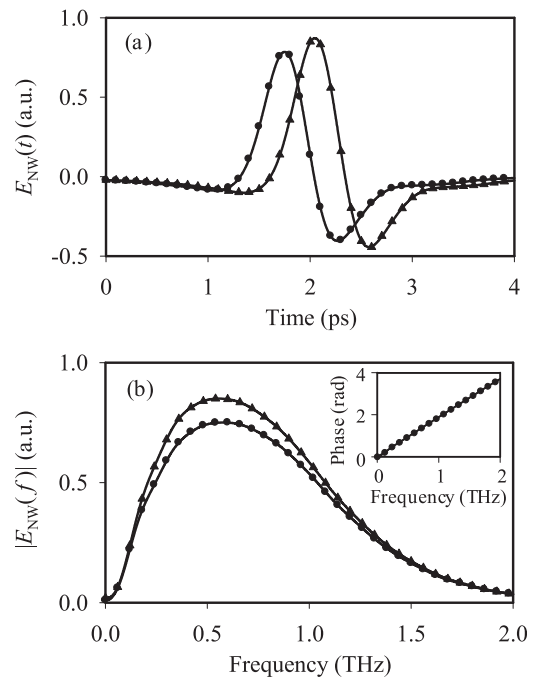

FIG. 2. (a) Measured (symbols) and calculated (lines) THz pulses transmitted through the SiNW sample at incidence angles θ of 0° (circles) and 40° (triangles). (b) Amplitude spectra of the same transmitted THz pulses. The inset shows the phase difference between the transmitted THz pulses for $\theta = 0°$ and 40°.

complex conductivity tensor. Using this relationship, we obtained the effective complex conductivity of the bare Si substrate, as shown in Fig. 3(a). The real part of the conductivity, $\sigma_1(\omega)$, decreases monotonically with increasing frequency. On the other hand, the imaginary part of the
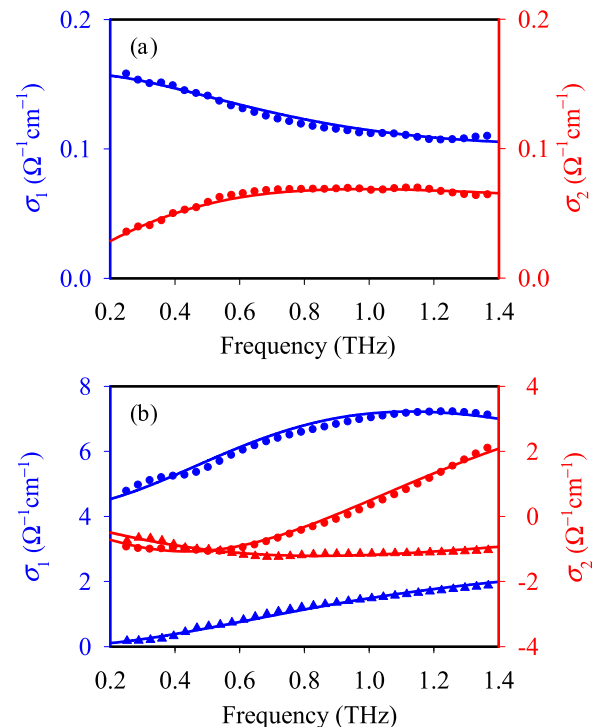

FIG. 3. Real (blue) and imaginary (red) conductivities of (a) bare Si substrate and (b) SiNW film. The transverse and longitudinal conductivities are represented by circles and triangles, respectively. The symbols and the lines stand for the experimental data and the calculation results, respectively.

conductivity, $\sigma_2(\omega)$, has a broad peak between 0.6 and 1.2 THz. This frequency dependence is usually observed in a Drude-like material. However, we used the Cole-Davidson (CD) model, which is a modified version of the simple Drude model, and is obtained by inserting a fractional exponent β because the Si substrate used in this work has a carrier density which is lower than $10^{16}\,\text{cm}^{-3}$.[22] The complex conductivity in the CD model is expressed as

$$\sigma_{CD}(\omega) = \frac{\omega_p^2 \varepsilon_0 \tau}{(1 - i\omega\tau)^\beta}, \qquad (2)$$

where ω_p is the plasma frequency and τ is the relaxation time. As shown in Fig. 3(a), the conductivity of the bare Si substrate is described well by the CD model with $\beta = 0.75$, which agrees with a previous report that p-type silicon has $\beta = 0.7$ at the low carrier density limit.[22]

Figure 3(b) shows the transverse and longitudinal complex conductivities of the SiNW film. In particular, the real part of the transverse conductivity of the SiNW film was much larger than that of the Si substrate. This was attributed to the presence of the residual Au film, which can significantly increase the conductivity of the SiNW film. The real parts of both the transverse and longitudinal conductivities of the SiNW film, denoted by $\sigma_1^T(\omega)$ and $\sigma_1^L(\omega)$, respectively, gradually increase with the frequency up to 1 THz; however, this is not observed for the case of the bare Si substrate when modeled using the Drude model. Also, the frequency dependence of $\sigma^T(\omega)$ is completely different to that of $\sigma^L(\omega)$. To explain these different frequency dependencies, we used two dispersion models, the DS and Lorentz models, for $\sigma^T(\omega)$ and $\sigma^L(\omega)$, respectively; the calculation results obtained from these models are in excellent agreement with the measurements, as shown in Fig. 3(b).

The DS model is a generalized form of the Drude model, obtained by using the impulse response approach combined with Poisson statistics.[23] The complex conductivity in the DS model is given by

$$\sigma_{DS}(\omega) = \frac{\omega_p^2 \varepsilon_0 \tau}{1 - i\omega\tau}\left[1 + \frac{c}{(1 - i\omega\tau)^p}\right], \qquad (3)$$

where c represents the fraction of the electron's original velocity that is retained after the collision. In Eq. (3), we used a single-scattering approximation, in which the velocity persistence is retained for only a single collision, with an additional fitting parameter p. In the DS model, unlike in the simple Drude model, the maximum real part of the conductivity is not at the zero frequency. Thus, the measured transverse conductivity of the SiNW film can be described using the DS model. From the least-squares fitting, we obtained the DS parameters given by $c = -0.70$ and $p = 0.97$ with $\omega_p/2\pi = 5.98$ THz and $\tau = 113.9$ fs. This indicates that the backscattering is significant for the transverse conductivity, and, more interestingly, that the single-scattering approximation ($p = 1$) is actually appropriate for the SiNW film.

The measured longitudinal conductivity of the SiNW film can also be described using the DS model. In the DS model with $c = -1$, the DC conductivity is suppressed and

the maximum real part of the conductivity occurs at $\omega\tau_0 = 1$, which leads to a Lorentz-like model.[8,23] The measured longitudinal conductivity of the SiNW film agrees well with the results of the DS model with $c \sim -1$ and $p = 0.5$. In this case, p is a fractional number and is treated as a disposable parameter without any obvious physical origin. We therefore used the Lorentz model for the longitudinal conductivity of the SiNW film. The longitudinal conductivity based on the Lorentz model is given by

$$\sigma_{LR}(\omega) = \frac{i\varepsilon_0 \omega_p^2 \omega}{\omega^2 - \omega_0^2 + i\omega/\tau}, \qquad (4)$$

where ω_0 is the resonant frequency. From the best-fit curves, we obtained $\omega_0/2\pi = 2.42$ THz, $\omega_p/2\pi = 5.42$ THz, and $\tau = 23.6$ fs.

The plasma frequency is defined by $\omega_p^2 = Nq^2/(m^*\varepsilon_0)$, where N is the hole density, q is the electron charge, and m^* is the effective mass. The measured transverse and longitudinal plasma frequencies of the SiNW film were $\omega_p/2\pi = 5.98$ THz and 5.42 THz, respectively, which are much larger values than that of the Si substrate, i.e., 0.47 THz. Because ω_p^2 is proportional to N/m^*, SiNWs can be considered to have a larger N/m^* value than the bare Si, at least in a phenomenological sense. Although thin nanowires generally exhibit some quantum confinement effects in terms of carrier density and effective mass,[24] it is unlikely that this quantum confinement enhances the conductivity of the SiNW film; this is because the diameter of the SiNWs in this work is $\sim$90 nm, which is too large to result in any significant quantum confinement effects. It is more likely that the large discrepancy between the plasma frequencies of the SiNWs and the bulk Si is because of the residual Au film, which has a high plasma frequency of $\sim$2000 THz. The relaxation time for the longitudinal conductivity of the SiNWs was nine times smaller than that of the bulk Si, probably because of surface defects that were introduced in the SiNWs during the etching process.

In summary, we measured the THz complex conductivity tensor of a highly anisotropic SiNW film using a high-precision THz-TDS system. We then used the Drude-Smith and Lorentz models to analyze the transverse and longitudinal conductivities of the SiNW film, respectively. The THz measurements were found to be in excellent agreement with the results of the calculations based on these models. The highly anisotropic properties of these SiNW films are expected to find many applications in polarization-sensitive devices and components, such as polarizers, detectors, and metamaterials, at THz frequencies.

[1]Y. Huang, X. Duan, Y. Cui, L. J. Lauhon, K. Kim, and C. M. Liever, Science **294**, 1313 (2001).
[2]Y. Cui, Q. Wei, H. Park, and C. M. Liever, Science **293**, 1289 (2001).
[3]A. I. Boukai, Y. Bunimovich, J. Tahir-Kheli, J. Yu, W. A. Goddard III, and J. R. Heath, Nature (London) **451**, 168 (2008).

[4]V. Sivakov, G. Andra, A. Gawlik, A. Berger, J. Plentz, F. Falk, and S. H. Christiansen, Nano Lett. **9**, 1549 (2009).

[5]G. B. Jung, Y. J. Cho, Y. Myung, H. S. Kim, Y. S. Seo, J. Park, and C. Kang, Opt. Express **18**, 16353 (2010).

[6]J. B. Baxter and C. A. Schmuttenmaer, J. Phys. Chem. B **110**, 25229 (2006).

[7]H. Ahn, Y.-P. Ku, Y.-C. Wang, C.-H. Chuang, S. Gwo, and C.-L. Pan, Appl. Phys. Lett. **91**, 163105 (2007).

[8]P. Parkinson, J. Lloyd-Hughes, Q. Gao, H. H. Tan, C. Jagadish, M. B. Johnston, and L. M. Herz, Nano Lett. **7**, 2162 (2007).

[9]J. H. Strait, P. A. George, M. Levendorf, M. Blood-Forsythe, F. Rana, and J. Park, Nano Lett. **9**, 2967 (2009).

[10]M. Brucherseifer, M. Nagel, P. H. Bolivar, H. Kurz, A. Bosserhoff, and R. Buttner, Appl. Phys. Lett. **77**, 4049 (2000).

[11]E. Jung, J. Kim, Y. Han, K. Moon, M. Lim, and H. Han, Biochip J. **2**, 296 (2008).

[12]M. Cho, J. Kim, H. Park, Y. Han, K. Moon, E. Jung, and H. Han, Opt. Express **16**, 7 (2008).

[13]T. Hofmann, C. M. Herzinger, A. Boosalis, T. E. Tiwald, J. A. Woollam, and M. Schubert, Rev. Sci. Instrum. **81**, 023101 (2010).

[14]T. Nagashima and M. Hangyo, Appl. Phys. Lett. **79**, 3917 (2001).

[15]N. Matsumoto, T. Hosokura, T. Nagashima, and M. Hangyo, Opt. Lett. **36**, 265 (2011).

[16]T. Hofmann, C. M. Herzinger, J. L. Tedesco, D. K. Gaskill, J. A. Woollam, and M. Schubert, Thin Solid Films **519**, 2593 (2011).

[17]P. Boher, J. P. Piel, and B. Sacepe, Thin Solid Films **455–456**, 581 (2004).

[18]T. Hofmann, D. Schmidt, A. Boosalis, P. Kuhne, R. Skomski, C. M. Herzinger, J. A. Woollam, M. Schubert, and E. Schubert, Appl. Phys. Lett. **99**, 081903 (2011).

[19]Z. Huang, N. Geyer, P. Werner, J. Boor, and U. Gosele, Adv. Matt. **23**, 285 (2011).

[20]A. Sihvola, *Electromagnetic Mixing Formulas and Applications* (The Institution of Engineering and Technology, London, 2008).

[21]H. Fujiwara, *Spectroscopic Ellipsometry: Principles and Applications* (John Wiley & Sons, England, 2007), p. 224.

[22]T.-I. Jeon and D. Grischkowsky, Appl. Phys. Lett. **72**, 2259 (1998).

[23]N. V. Smith, Phy. Rev. B **64**, 155106 (2001).

[24]Y. Zheng, C. Rivas, R. Lake, K. Alam, T. B. Boykin, and G. Klimeck, IEEE Trans. Electron Devices **52**, 1097 (2005).